The Structure of Interlayer Water in Li−Montmorillonite Studied by Neutron Diffraction with Isotopic Substitution

D. Hugh Powell*

Institut de Chimie Minérale et Analytique, Université de Lausanne-BCH, CH-1015 Lausanne, Switzerland

Henry E. Fischer

Institut Laue Langevin, Avenue des Martyrs, BP 156, 38042 Grenoble Cedex 9, France

Neal T. Skipper

Department of Physics & Astronomy, University College, London, Gower Street, London WC1E 6BT, U.K.

Received: July 10, 1998; In Final Form: November 2, 1998

We used neutron diffraction with an incident wavelength of 0.5024 Å and both H/D and ^{6}Li/^{nat}Li isotopic substitution to study the structure of interlayer water in Li−Wyoming montmorillonite hydrates, with water contents corresponding to two-layer hydrates. The hydrogen isotope first-order difference gives the weighted sum of partial structure factors and radial distribution functions related to the intra- and intermolecular structure around interlayer water hydrogens. The results show unequivocally that the interlayer water adopts a liquid-type structure and that the clay surface does not prevent the interlayer water from adopting a highly hydrogen-bonded configuration. The lithium isotope first-order differences for D_2O and H_2O hydrates, and for the dry clay, are complicated by the presence of residual Bragg peaks. We discuss the possible origins of these features and the prospects for the further application of this technique to the study of hydrated clays.

Introduction

The understanding of the structure of the interlayer region of swelling clays such as smectites (of which montmorillonite is a member) and vermiculites is fundamental to clay science. These clays consist of negatively charged silicate layers held together by cations to give a stacked (crystalline) structure (Figure 1). The hydration of interlayer cations and the clay surface controls the swelling, dispersion, and ion exchange properties of the clays, and it is an important part of the clays' usability in catalysts, waste disposal, and other applications.[1−4]

There have been considerable advances in the use of computer simulations to study interlayer structure in both smectites and vermiculites.[5−8] The vermiculite studies have advanced in tandem with neutron diffraction experiments.[9−11] The fact that vermiculites form well-defined macroscopic crystals allows accurate sample orientation, so that scattering density profiles across the interlayer region perpendicular to the clay layers can be obtained and detailed models of the interlayer structure constructed. The relatively disordered structure of the technologically and environmentally more important smectites makes them difficult to study using this approach. The properties of smectites cannot simply be inferred from the properties of vermiculites: smectites have 2−3 times lower charge density than vermiculites, and in the case of the Wyoming montmorillonite studied here, most of the charge is due to isomorphic substitutions in the octahedral layer at the center of the clay sheets, whereas for vermiculite the charge is sited in the tetrahedral layers nearer the clay surface (Figure 1).

We have tried to overcome the difficulties associated with performing crystallographic studies of montmorillonites in recent neutron diffraction studies of powdered Na− and Li−montmorillonite D_2O hydrates by adopting an approximate difference method with the dry clay as the reference.[12,13] This method allowed us to separate, to a good approximation, the diffuse diffraction pattern due to interlayer water from the Bragg diffraction due to the crystalline structure of the aluminosilicate layers. The results show qualitatively that the interlayer water has a liquidlike structure. However, the approximate nature of this method limits the possibility to study the small structural differences that would be evidence, for instance, of disruption of the water hydrogen-bonding networks due to interactions with the clay surface. The neutron diffraction isotopic difference method, which is widely applied in the study of multicomponent liquid and amorphous structures, offers an exact approach for separating the diffuse (liquid) diffraction from the Bragg (crystal) diffraction characteristic of the clays.

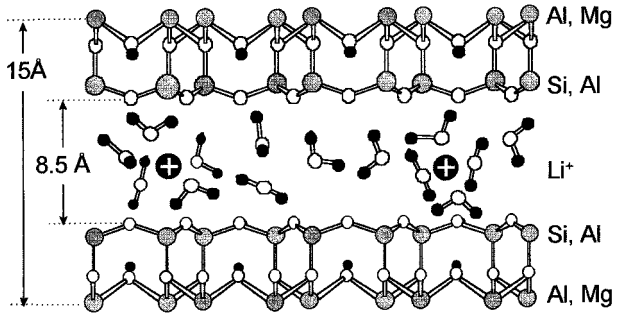

Figure 1. Schematic cross-section perpendicular to the clay layers in Li-montmorillonite, showing the layers of octahedrally (Al, Mg) and tetrahedrally (Si, Al) coordinated cations and the interlayer cations and water (hypothetical interlayer structure): (○) oxygen atoms, (●) hydrogen atoms. The dimensions shown are for the two-layer hydrate.

We present here a study of Li−montmorillonite hydrates using both H/D and ^{6}Li/^{nat}Li isotopic substitution in the

10.1021/jp982966r CCC: $15.00
Published on Web 12/08/1998

TABLE 1: Compositions of the Six Li−Montmorillonite (SWy2) Samples and the Effective Densities and Neutron Cross Sections Used in the Data Correction Procedures

sample	^{6}Li−SWy2 dry	^{nat}Li−SWy2 dry	^{6}Li−SWy2 14.5% D_2O	^{nat}Li−SWy2 14.5% D_2O	^{6}Li−SWy2 14.8% H_2O	^{nat}Li−SWy2 14.8% H_2O
c_O			0.104	0.104	0.113	0.113
c_H or c_D			0.208	0.208	0.227	0.227
c_{H2}	0.098	0.098	0.068	0.068	0.065	0.065
c_{O2}	0.589	0.589	0.405	0.405	0.389	0.389
c_{Li}	0.018	0.018	0.013	0.013	0.012	0.012
c_{Mg}	0.012	0.012	0.008	0.008	0.008	0.008
c_{Al}	0.092	0.092	0.063	0.063	0.061	0.061
c_{Si}	0.190	0.190	0.131	0.131	0.126	0.126
$\overline{M_r}$	17.76	17.76	14.30	14.32	13.76	13.77
ρ_{eff} (g cm^{-3})	0.750	0.582	0.907	0.746	0.849	0.695
σ_S (barn)	5.17	5.18	4.77	4.78	8.65	8.66
σ_a (barn) at 0.5024 Å	4.85	0.39	3.34	0.27	3.22	0.28

interlayer. We studied water contents corresponding to the so-called two layer hydrates: these are conventionally pictured as two water monolayers between the clay sheets, although the water structure is certainly more complicated. The hydrogen isotopic substitution offers the possibility of studying the detailed water structure. The lithium isotopic substitution can be used to study the lithium coordination environment: if the Li−O and Li−H or Li-D peaks in the first coordination shell are resolvable, the ratio of the integrals of these peaks could be used as a test for the presence of innersphere complexes of Li^+ with the clay surface, i.e., of direct binding of Li^+ to the clay surface.

Experimental Section

The Wyoming montmorillonite (Clay Minerals Society source clay SWy-2) was purified first by suspending ca. 40 g of the raw clay with 125 cm^3 of 1 M NaCl followed by dialysis to remove excess salt (the $AgNO_3$ test was used to verify the absence of Cl^- in the dialyte). This ion-exchange procedure was repeated. The >2 μm size fraction, which contains quartz and other impurities, was then removed by sedimentation. The purified sample was oven dried at 100 °C then lightly ground in a mortar prior to undergoing ion exchange with Li^+. Enriched ^{6}Li metal (95%, 1.54 g, Isotec, Inc.) was dissolved piece-by-piece in deionized water: the resulting ^{6}LiOH solution was neutralized with HCl to produce 250 cm^3 of 1.02 M ^{6}LiCl solution with pH $\sim$ 5.5. A pH $\sim$ 5.5 solution of ^{nat}LiCl (92.5% ^{7}Li, 7.5% ^{6}Li) was prepared from LiCl salt (Analar) and deionized water. Two 13 g portions of the purified Na−montmorillonite were converted to the ^{6}Li and ^{nat}Li forms, respectively, by suspending the clay for 1 day in ca. 80 cm^3 portions of the LiCl stock solutions made up to around 200 cm^3 with distilled water, dialyzing to remove excess ions then oven drying at 100 °C. The exchange process was repeated three times. The resulting oven dried ^{6}Li− and ^{nat}Li−montmorillonites were ground lightly in a mortar, then dried under vacuum at 100 °C. X-ray diffraction of the treated powder samples and the untreated clay did not show any evidence of change of the crystal structure of the clay during treatment, but did show that most of the quartz impurity had been removed. About 3 g of each sample was equilibrated with ca. 10 cm^3 saturated solution of KI in distilled water in a ca. 400 cm^3 plastic container: this saturated solution produces a relative humidity of 69% at 25 °C. The clay samples were weighed at regular intervals over a period of 16 days. At the end of the period the water content of the clays had stabilized at 148 $\pm$ 5 mg/g water per total weight of clay. About 2 days were necessary to reach half this final water content. This observation is of practical importance: the hydration/dehydration process takes place on the time scale of days, so the hydration state will not be influenced by exposure of the samples to a dry atmosphere for a few minutes while transferring from one container to another.

The remainder of the ^{6}Li and ^{nat}Li samples were equilibrated with 99.96% pure D_2O (ICN Biomedical) over a period of 1 day, then redried under vacuum at 120 °C: all manipulations where the clays or D_2O were exposed to the atmosphere were performed in a dry glovebox. About 3 g of each sample was then equilibrated with ca. 10 cm^3 saturated solution of KI in D_2O, where the KI had been dried under vacuum at 150 °C. After 12 days of equilibration the D_2O contents of the samples had stabilized at 145 $\pm$ 5 mg/g D_2O per total weight of clay. The samples were sealed in airtight plastic containers for transport to the Institut Laue Langevin (see below). All subsequent manipulations of the dry and D_2O containing samples were performed in a dry glovebox. The hydrated samples were left to equilibrate with the appropriate saturated solutions of KI until transfer to the sample container for the neutron experiments. The compositions of the different samples, assuming a simplified formula for the dry clay—$Li_{0.75}(Si_{7.75}Al_{0.25})(Al_{3.5}Mg_{0.5})O_{20}(OH)_4$—are given in Table 1. The final water contents of each ^{6}Li/^{nat}Li pair were identical within error. The water contents correspond to 7.0 $\pm$ 0.2 H_2O and 6.15 $\pm$ 0.2 D_2O per formula unit above: this is consistent with so-called two-layer hydrates, although some one- and three-layer hydrates are certainly present.[14] The lower water content of the D_2O hydrates, compared to the H_2O hydrates, may be a result of the additional drying treatment that the deuterated batches received.

The neutron diffraction measurements were performed on the D4 diffractometer on the steady-state neutron source of the Institut Laue Langevin, France. The incident wavelength was 0.5024 Å, measured using a Ni powder reference. We chose to use this relatively low wavelength compared to the more intense 0.71 Å wavelength available on the diffractometer in order to reduce the absorption cross section of ^{6}Li and the scattering cross section of H_2O (with increasing neutron energy the scattering cross section of H changes from its bound value of 82 barn to its free atom value of 20.5 barn: 1 barn = 100 fm^2). The shorter wavelength also reduces the size of the corrections necessary for inelasticity effects due to scattering from light atoms in the samples. The samples were contained in a 6.7 mm i.d., 7.0 mm o.d. cylindrical vanadium container sealed with a metallic O-ring. The loaded sample container was weighed before and after each measurement to verify that no dehydration had occurred due to inadequate sealing of the container. Diffraction patterns were measured at ambient temperature (298 K) for each of the samples, for liquid D_2O, the empty sample container, the instrument background and a 6.08 mm diameter Vanadium rod. The data were corrected for background, empty

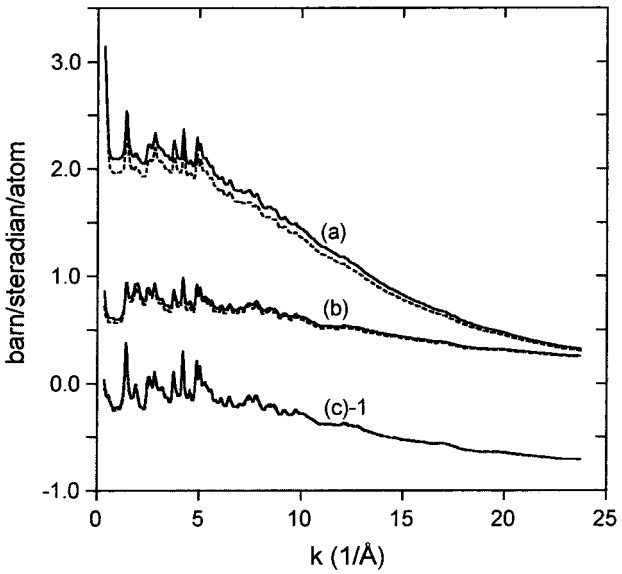

Figure 2. Normalized neutron diffraction patterns $I^m(k)$ for ^{6}Li−montmorillonite (solid lines) and ^{nat}Li-montmorillonite (dashed lines) (a) in the H_2O hydrated form, (b) in the D_2O hydrated form, and (c) the vacuum-dried state.

container, attenuation,[15] and multiple scattering,[16] normalized to the scattering from a vanadium rod[17] and rebinned into k intervals of 0.05 Å^{-1}, where the modulus of the scattering vector $k = 4\pi\sin\theta/\lambda$. The scattering and absorption cross sections, σ_S and σ_a, of the samples were calculated using, apart from for H and D, the elemental cross sections given in Sears' tables.[18] Based on the measured total cross sections for 0.5024 Å neutrons,[19] σ_T (H_2O) = 46.2 barn molecule^{-1} and σ_T (D_2O) = 11.7 barn molecule^{-1}, we used scattering cross-sections per atom for H and D of 21 barn and 3.7 barn, respectively. The atomic densities used in the data analysis were calculated from the effective mass densities, ρ_{eff} (weight of sample divided by volume of container) and the mean atomic weights $\bar{M}_r$ given in Table 1.

Results and Discussion

The corrected, normalized intensities $I(k)$ for the six Li−montmorillonites are shown in Figure 2. These functions are given, within the static approximation[20] and for isotropic samples, by

$$I(k) = \sum_\alpha c_\alpha b_\alpha^2 + F(k) \quad (1)$$

where c_α is the atomic fraction, and $\overline{b_\alpha^2}$ the mean square scattering length of species α, and the scattering factor $F(k)$, given by

$$F(k) = \sum_\alpha \sum_\beta c_\alpha c_\beta b_\alpha b_\beta [S_{\alpha\beta}(k) - 1] \quad (2)$$

where b_α is the mean coherent scattering length of species α and $S_{\alpha\beta}(k)$ are the partial structure factors. In practice the first "self-scattering" term in eq 1 is k-dependent due to recoil effects in scattering from light nuclei (primarily H and D) leading to the downward slope on the $I(k)$ with increasing k. We therefore denote the measured corrected intensities $I^m(k)$ to differentiate them from the true $I(k)$ defined by eq 1. The $F(k)$ is dominated in all cases by Bragg scattering although, as we showed in

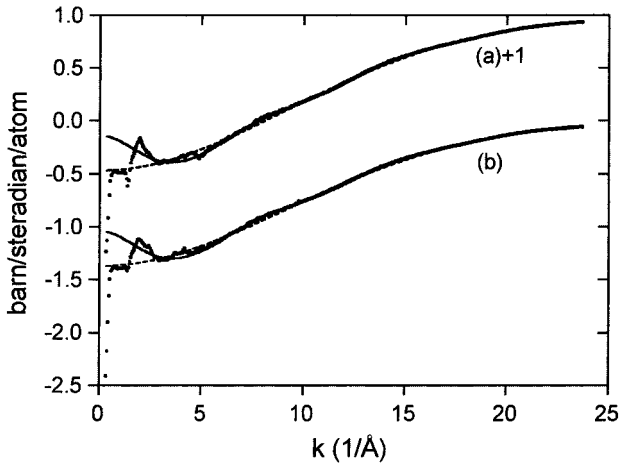

Figure 3. The difference function $\Delta_H^m(k)$ for (a) ^{6}Li−montmorillonite and (b) ^{nat}Li−montmorillonite with fitted self-scattering background (dashed lines) and background plus molecular form factor (solid lines).

TABLE 2: Weighting Factors of the Different $S_{H\alpha}(k)$ and $g_{H\alpha}(r)$ in the D/H First-Order Difference Functions and Their Fourier Transforms (Calculated Using the Neutron-Scattering Lengths Compiled by Sears[18])

	^{6}Li−SWy2	^{nat}Li−SWy2
$2c_Hc_O(b_D-b_H)b_O$	28.7 mbarn	28.7 mbarn
$c_H^2(b_D^2-b_H^2)$	14.5 mbarn	14.5 mbarn
$2c_Hc_{H2}(b_D-b_H)b_H$	−11.2 mbarn	−11.2 mbarn
$2c_Hc_{O2}(b_D-b_H)b_O$	104.4 mbarn	104.4 mbarn
$2c_Hc_{Li}(b_D-b_H)b_{Li}$	1.1 mbarn	−1.1 mbarn
$2c_Hc_{Mg}(b_D-b_H)b_{Mg}$	2.0 mbarn	2.0 mbarn
$2c_Hc_{Al}(b_D-b_H)b_{Al}$	9.7 mbarn	9.7 mbarn
$2c_Hc_{Si}(b_D-b_H)b_{Si}$	24.1 mbarn	24.1 mbarn
total = $-G_H(0)$	173.3 mbarn	171.1 mbarn

previous publications,[12,13] there is a significant diffuse component for the hydrates due to the interlayer water.

If the compositions of two samples are identical except for the substitution of the isotope of an element X, subtracting one $I(k)$ from the other will give, within the static approximation, the first-order difference function

$$\Delta_x(k) = c_x(\overline{b_x^2} - \overline{b_{x'}^2}) + c_x^2(b_x^2 - b_{x'}^2)[S_{xx}(k) - 1] + \sum_{\alpha\neq X} 2c_xc_\alpha(b_x - b_{x'})b_\alpha[S_{x\alpha}(k) - 1] \quad (3)$$

where X and X′ refer to the two different isotopes. All partial structure factors not involving element X are eliminated. On the basis of our previous studies,[12,13] we can expect that for H/D substitution in our clays this will mean elimination of the Bragg scattering to produce a diffuse pattern related to the H−water and H−clay correlations. The measured $\Delta_H^m(k)$ for the ^{6}Li and ^{nat}Li samples are shown in Figure 3. The residual Bragg peaks in the two functions are very small: the fact that they are inverted in the ^{nat}Li−montmorillonite data suggests that they are the results of experimental error (see below) rather than of any real periodicity in the H-clay correlations. In our previous experiments,[12,13] we used an approximate method to show that the interlayer water diffraction was diffuse: these more exact isotopic substitution measurements confirm this result. Neglecting error terms due to the slightly different water contents of the H_2O and D_2O hydrates and taking average values for c_O and c_H, the weighting factors in eq 3 are those given in Table 2.

To obtain real-space information via Fourier transformation one must first obtain the true $\Delta_H(k)$ from the measured $\Delta_H^m(k)$

TABLE 3: Parameters Obtained by Fitting a Molecular Form Factor and Background Function to the Measured $\Delta_H^m(k)$ for ^{6}Li− and ^{nat}Li−montmorillonite and the $I(k)$ for D_2O Measured under the Same Conditions

	^{6}Li−SWy2	^{nat}Li−SWy2	D_2O
d_{OH} (Å)		0.963 ± 0.002	0.972 ± 0.003
γ_{OH} (Å^2)		0.074 ± 0.002	0.081 ± 0.007
d_{HH}(Å)		1.44 ± 0.05	1.50 ± 0.03
γ_{HH}(Å^2)		0.23 ± 0.02	0.16 ± 0.02
A (barn sr^{-1} atom^{-1})	-0.0188 ± 0.0008	-0.0139 ± 0.0008	
C_G (barn sr^{-1} atom^{-1})	-1.4516 ± 0.0009	-1.3573 ± 0.0009	
W_G (Å^{-2})	9.158 ± 0.009	9.157 ± 0.009	

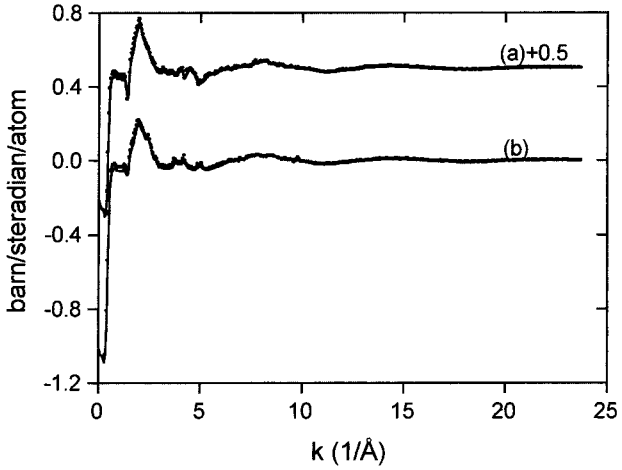

Figure 4. The corrected interference components of the D/H first-order difference functions $\Delta_H(k)$ for (a) ^{6}Li−montmorillonite and (b) ^{nat}Li−montmorillonite. The points are the corrected data and the solid lines are minimum noise fits.

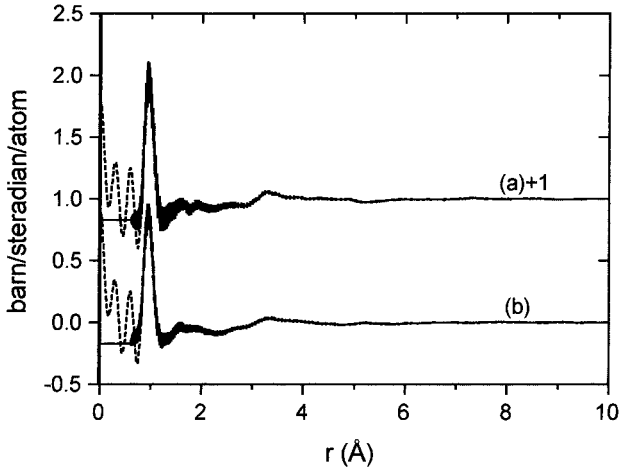

Figure 5. The real-space first-order difference functions $G_H(r)$ for (a) ^{6}Li−montmorillonite and (b) ^{nat}Li−montmorillonite obtained by Fourier transformations of the unsmoothed data (dashed lines) and from minimum noise fits (solid lines with error bars).

by correcting for the k-dependence of the self-scattering component of the diffraction. It is generally necessary to resort to some semiempirical correction method. We chose to describe the self-scattering background by a Gaussian and a constant

$$\mathrm{BACK}(k) = A + C_G \exp\left\{-\frac{k^2}{2W_G^2}\right\} \quad (4)$$

with three fit parameters A, C_G, and the width W_G. The parameters that best describe the data in the range $k > 5$ Å^{-1} are given in Table 3. The fitted functions are shown as dashed lines in Figure 3.

Subtraction of the fitted BACK(k) from the $\Delta_H^m(k)$ yields the corrected difference functions $\Delta_H(k)$ in Figure 4. Fourier transformation of these functions leads to the real-space first-order difference function $G_H(r)$ defined by

$$G_x(r) = \frac{1}{2\pi^2\rho_n}\int_0^\infty [\Delta_x(k) - c_x(\overline{b_x^2} - \overline{b_{x'}^2})]k^2 \frac{\sin kr}{kr}\,\mathrm{d}k$$

$$= c_x^2(b_x^2 - b_{x'}^2)[g_{HH}(r) - 1] + \sum_{\alpha\neq H} 2c_x c_\alpha (b_x - b_{x'})b_\alpha [g_{X\alpha}(r) - 1] \quad (5)$$

where ρ_n is the atomic number density within the clay crystallites, i.e., independent of packing density. We estimated $\rho_n = 0.1$ Å^{-3} on the basis of the crystal structure of vermiculite hydrates.[21] The weighting factors of the partial pair distribution functions, $g_{H\alpha}(r)$ are as given in Table 2. The $G_H(r)$ for the ^{6}Li− and ^{nat}Li−montmorillonites are shown in Figure 5. As well as simple Fourier transformation, we also calculated $G_H(r)$ using a minimum-noise reconstruction technique:[22] the reconstructed k- and r-space functions are shown as smooth lines in Figures 4 and 5. The $G_H(r)$ are dominated by the intramolecular OH peak at 0.96 Å. With the approximation that only $g_{OH}(r)$ is important in this region, integration over the first peak gives the hydrogen−oxygen coordination number

$$n_H^O = 4\pi\rho_n c_O \int_0^{r_{min}} g_{OH}(r) r^2\,\mathrm{d}r \approx \frac{4\pi\rho_n c_O}{2c_H c_O(b_D - b_H)b_O}\int_0^{r_{min}} [G_H(r) - G_H(0)]r^2\,\mathrm{d}r \quad (6)$$

With r_{min} corresponding to the first minimum at ca. 1.3 Å, one obtains $n_H^O = 1.05 \pm 0.03$ and 1.02 ± 0.05 for the ^{6}Li− and ^{nat}Li− clays, respectively. The fact that these values are very close to the expected value of 1.0 indicates that the normalization of our data is good.

To remove the intramolecular contribution from $\Delta_H(k)$ we fitted the data with the molecular form factor

$$\mathrm{MFF}(k) = a_{OH}\frac{\sin(kd_{OH})}{kd_{OH}}\exp\left(-\frac{\gamma_{OH}^2 k^2}{2}\right) + a_{HH}\frac{\sin(kd_{HH})}{kd_{HH}}\exp\left(-\frac{\gamma_{HH}^2 k^2}{2}\right) \quad (7)$$

where $a_{OH} = 2c_H b_O(b_D - b_H)$, $a_{HH} = c_H(b_D^2 - b_H^2)$, d_{OH} and d_{HH} are the intramolecular interatomic distances, and γ_{OH} and γ_{HH} are factors similar to Debye−Waller factors that measure the vibrational amplitudes. We fitted the combined function BACK(k) + MFF(k) to the $\Delta_H(k)$ in the range $k > 5$ Å^{-1} to yield the fit parameters given in Table 3. The fitted functions are shown as solid lines in Figure 3. The parameters describing the intramolecular structure of the water molecule for the two clays are not significantly different from those obtained from a fit to the liquid D_2O diffraction pattern obtained with the same experimental conditions. If one subtracts the fitted molecular

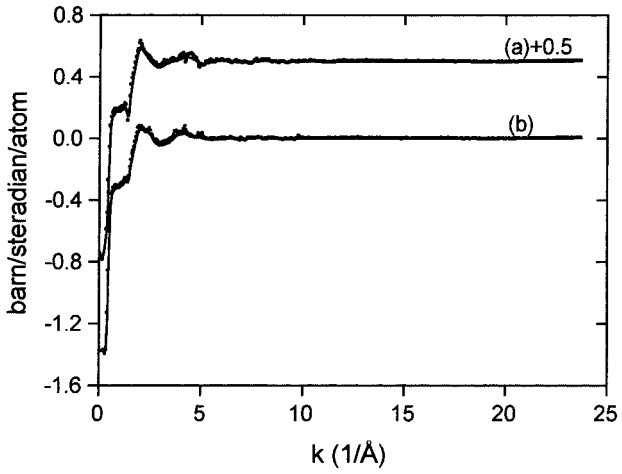

Figure 6. The intermolecular interference components of the D/H first-order difference functions $\Delta_H^{inter}(k)$ for (a) ^{6}Li−montmorillonite and (b) ^{nat}Li−montmorillonite. The points are the data and the solid lines are minimum noise fits.

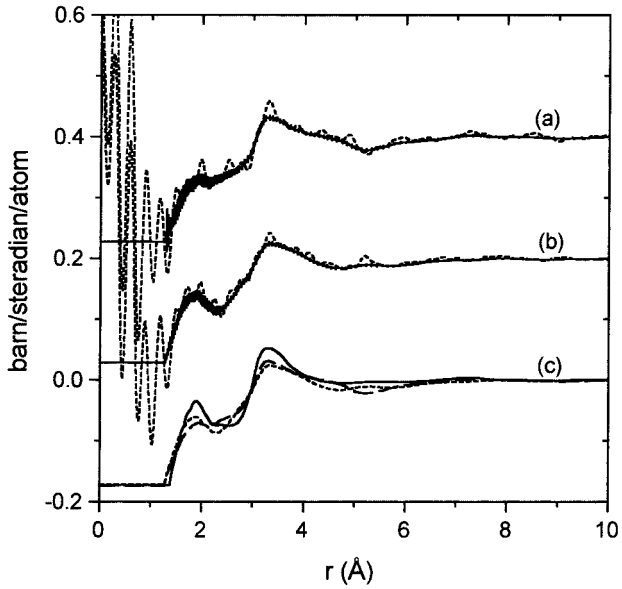

Figure 7. The real-space intermolecular first-order difference functions $G_H^{inter}(r)$ for (a) ^{6}Li−montmorillonite and (b) ^{nat}Li−montmorillonite obtained by Fourier transformations of the unsmoothed data (dashed lines) and from minimum noise fits (solid lines with error bars). In (c) the minimum noise fits for ^{6}Li−montmorillonite (long dashed curve) and ^{nat}Li−montmorillonite (short-dashed curve) are compared with the function $G_H^{water}(r) = 3.98[0.0287(g_{HO}(r) - 1) + 0.0145(g_{HH}(r) - 1)]$ for liquid water calculated from the data of Soper et al.[23]

form factor, MFF(k) from the $\Delta_H(k)$ one obtains the intermolecular difference function $\Delta_H^{inter}(k)$ defined by eq 3 but with the intramolecular components of the $S_{HO}(k)$ and $S_{HH}(k)$ removed. The interference components of these functions are shown in Figure 6. Fourier transformation using eq 5 or minimum-noise reconstruction yields the intermolecular difference function $G_H^{inter}(r)$ in Figure 7. Like $G_H(r)$, $G_H^{inter}(r)$ is defined by eq 5, but the intramolecular O−H and H−H peaks centered at d_{OH} and d_{HH} no longer appear and the intermolecular structure is better defined (compare Figures 5 and 7). We expect the immediate environment of the interlayer water hydrogen to be dominated by water−water correlations and possibly interactions with the oxygens of the clay surface. It is therefore valid to compare with an appropriately weighted combination of the $g_{HO}(r)$ and $g_{HH}(r)$ for liquid water. In Figure 7 we show the function $G_H^{water}(r) = 3.98[0.0287(g_{HO}(r) - 1)+0.0145(g_{HH}(r) - 1)]$ calculated from a recent study of liquid water[23] where the factor 3.98 gives a $G_H(0)$ value close to that of the clays. The similarity of the three functions is striking, and indicates that the immediate coordination environment of a water molecule in the interlayer is similar to that in liquid water and certainly resembles liquid water more than any ice structure.[24] The peak at ca. 1.8 Å corresponds to the hydrogen-bond length. Integration over this peak according to eq 6 with $r_{min} = 2.25$ Å gives an intermolecular $n_H^O = 1.09 \pm 0.05$ for liquid water and 1.30 ± 0.05 and 1.37 ± 0.05 for the ^{6}Li− and ^{nat}Li−montmorillonites, respectively. For liquid water a value of 1.0 would be the maximum for hydrogen-bonded networks with every H-atom bonding to a neighboring oxygen. The fact that a larger value is obtained indicates some error due to peak overlap. The fact that a similar value is obtained for the clays indicates that there is little or no reduction of hydrogen bonding. While we cannot determine from these data whether some water molecules hydrogen bond to the oxygens of the clay surface, it is certain that such water−clay interactions do not prevent the interlayer water molecules from forming networks with near the maximum of four hydrogen bonds per molecule.

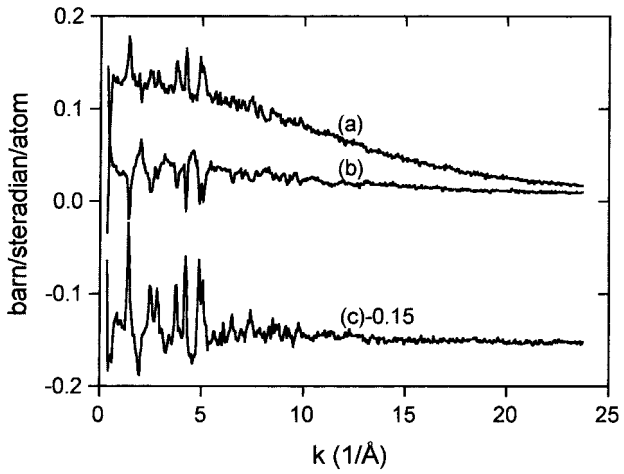

Figure 8. The measured Li first-order difference functions $\Delta_{Li}^m(k)$ for Li−montmorillonite (a) H_2O hydrate, (b) D_2O hydrate, and (c) vacuum dried.

We now turn our attention to the lithium isotope substitution. Subtraction of the ^{nat}Li−montmorillonite data from the ^{6}Li−montmorillonite data in the dry state, in the H_2O hydrates, and in the D_2O hydrates gives the data in Figure 8. These functions are described in theory by eq 3 with X = Li. It can be seen that the residual Bragg peaks in these functions are significant. If these peaks were due to Li−clay correlations they would be similar for all three difference functions: the fact that they are inverted for the D_2O hydrate compared to the dry clay and the H_2O hydrate means that they must instead be due to experimental error. The size of the residual Bragg peaks is around 10% of the size of the peaks in the original $I^m(k)$. One might suppose that the residual Bragg peaks are due to an error in the relative normalization of the ^{6}Li and ^{nat}Li samples. We therefore attempted to remove the residual Bragg peaks in the D_2O hydrate data by scaling the ^{nat}Li−montmorillonite $I(k)$ in the difference. The difference $I^6(k) - 0.85I^{nat}(k)$ shown in Figure 9 produces near perfect cancellation of the Bragg peaks. However, the resulting difference function resembles a D_2O diffraction pattern, and is too large by around an order of magnitude to be the true isotope difference. Fourier transformation of the difference function gives a strong positive peak at ca. 1 Å, the magnitude of which allows us to estimate that about 20% of the interlayer D_2O pattern is contaminating the scaled

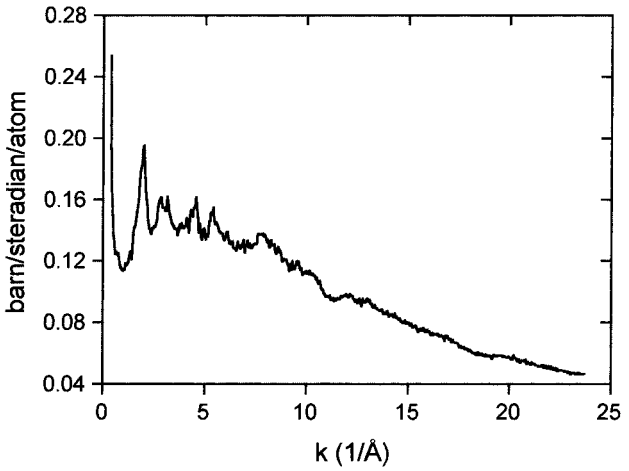

Figure 9. The scaled Li first-order difference function, $\Delta_{Li}{}^{m}(k) = I^{6}(k) - 0.85I^{nat}(k)$ for Li−montmorillonite D_2O hydrate. Note that the first peak at around 1.9 $Å^{-1}$ coincides with that in Figure 4.

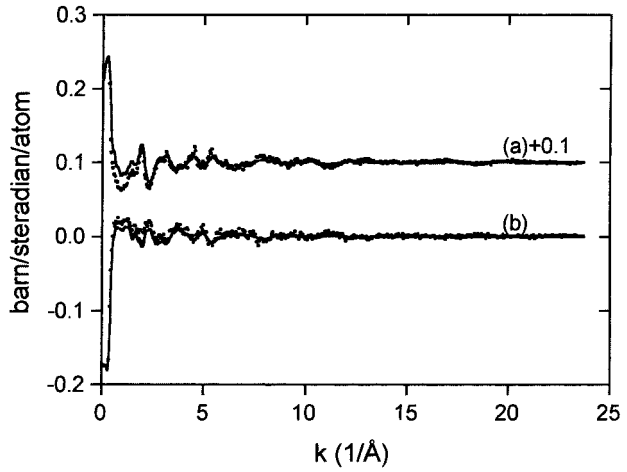

Figure 10. The interference components of the Li first-order difference functions $\Delta_{Li}(k)$ for (a) D_2O hydrated and (b) H_2O hydrated Li−montorillonite after correction for the residual Bragg peaks (see text). The points are the data and the solid lines are minimum noise fits.

difference function. This is clearly inconsistent with a simple scaling error. In addition, the precision of the intramolecular n_H^O found above would indicate than any scaling errors or differences in water content are less than 5%. Weighing during sample preparation showed that the water contents for each ^{6}Li/^{nat}Li pair are equal to within 3%. The data are thus consistent neither with a significant relative normalization error nor with a discrepancy in the sample compositions. A possible explanation for the residual Bragg peaks is that partial orientation of the clay samples leads to some irreproducibility of the Bragg component of the diffraction patterns. Montmorillonite crystallites are around 0.1 to 2 μ in diameter and consist on average of around seven platelets,[25] so that they are themselves platelike, with the short dimension ca. 0.01 μ perpendicular to the individual aluminosilicate sheets that make up each crystallite. The method of drying from suspension followed by crushing is likely to produce grains within which there is a preferential orientation of the individual crystallites, and which will also tend to be platelike. The process of filling the sample container may produce partial orientation of the grains as the powder settles, with the clay platelets tending to align horizontally, i.e., in the diffraction plane. This will reduce the intensities of the (00*l*) reflections and enhance the other Bragg peaks. It would be very difficult to correct for such an effect, but its importance could be reduced by rotating the sample or by averaging over a series of measurements between which the sample is removed from the can and reloaded.

For the present data, we can attempt to correct for the residual Bragg peaks in the $\Delta_{Li}(k)$ by adding or subtracting a fraction of the dry clay data, assuming that the residual peaks are due only to clay−clay correlations. We first made a 0.49:0.51 combination of the dry ^{6}Li− and ^{nat}Li−montmorillonite $I^m(k)$: this combination cancels out the Li−clay contributions (since $b_{6Li} = -1.05\ b_{natLi}$) leaving only the clay−clay terms and a very small Li−Li term. We then added 12% of this composite function to the $\Delta_{Li}(k)$ for the D_2O hydrates and subtracted 10% from that for the H_2O hydrates, to have as good cancelation of the Bragg peaks as possible. The resulting corrected $\Delta_{Li}(k)$, after removal of the self-scattering by subtraction of a Gaussian fit (eq 4), are shown in Figure 10. The corresponding *r*-space functions, $G_{Li}(r)$ obtained by minimum noise reconstruction are shown in Figure 11 (the $G_{Li}(r)$ obtained by Fourier transformation are very noisy and are not shown). The weighting factors of the different partial $g_{Li\alpha}(r)$ are given in Table 4. The peaks in $G_{Li}(r)$ at around 1.7 Å (D_2O hydrates) and 2.2 Å (H_2O hydrates) are in the region of the Li−O peak at 1.96 Å observed for Li hydration in aqueous solution.[26] The peak and dip at 2.6 Å correspond well with the Li−D distance of 2.50−2.55 Å observed in solution. Integration over these peaks gives coordination numbers $n_{Li}^O = 3.9$ and 6.1 and $n_{Li}^H = 7.3$ and 9.5, respectively, for the D_2O and H_2O hydrates (compared to n_{Li}^O from 3.2 to 6.0 in concentrated solutions[26]). Because of the subjective nature of our correction for the residual Bragg peaks, we do not wish to overinterpret the first-order difference functions. In particular, given the discrepancy between the n_{Li}^O and the Li−O distances obtained from the two $\Delta_{Li}(k)$, we cannot

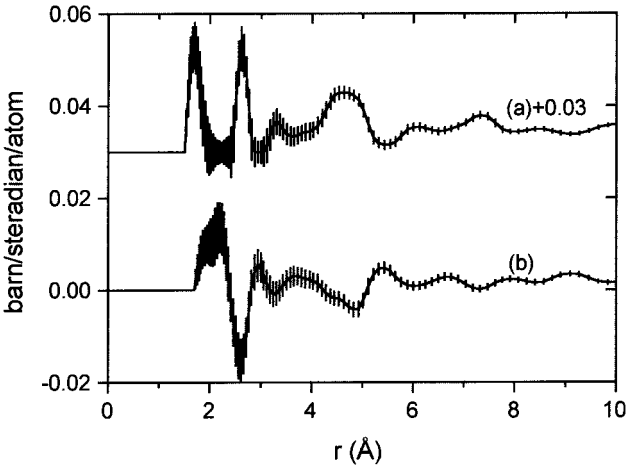

Figure 11. The real-space first-order difference functions $G_{Li}(r)$ for (a) D_2O hydrated and (b) H_2O hydrated Li−montorillonite obtained from minimum noise fits of the data in Figure 10.

TABLE 4: Weighting Factors of the Different $S_{Li\alpha}(k)$ and $g_{Li\alpha}(r)$ in the Li First−Order Difference Functions and Their Fourier Transforms (Calculated Using the Neutron-Scattering Lengths Compiled by Sears[18])

	$\Delta_{Li}{}^{D}(k)$	$\Delta_{Li}{}^{H}(k)$
$2c_{Li}c_O(b_6-b_{nat})b_O$	0.596 mbarn	0.623 mbarn
$2c_{Li}c_H(b_6-b_{nat})b_H$	1.370 mbarn	−0.803 mbarn
$2c_{Li}c_{H2}(b_6-b_{nat})b_H$	−0.250 mbarn	−0.229 mbarn
$2c_{Li}c_{O2}(b_6-b_{nat})b_O$	2.325 mbarn	2.137 mbarn
$c_{Li}2(b_62-b_{nat}2)$	0.001 mbarn	0.001 mbarn
$2c_{Li}c_{Mg}(b_6-b_{nat})b_{Mg}$	0.045 mbarn	0.041 mbarn
$2c_{Li}c_{Al}(b_6-b_{nat})b_{Al}$	0.216 mbarn	0.198 mbarn
$2c_{Li}c_{Si}(b_6-b_{nat})b_{Si}$	0.537 mbarn	0.493 mbarn
total $= -G_{Li}(0)$	4.840 mbarn	2.461 mbarn

take the fact that n_{Li}^{H} is slightly less than twice n_{Li}^{O} as evidence for the direct coordination of Li^+ to the clay surface. However, the fact that the coordination numbers obtained are of reasonable magnitude suggests that it will be possible to obtain reliable first-order difference data from interlayer cation isotopic substitution in montmorillonite, particularly for cations such as Ni^{2+} that have isotopes with a more favorable spread of neutron scattering lengths than lithium.

In conclusion, we have demonstrated that it is possible to apply the technique of isotopic substitution with first-order differences to crystalline clay samples in order to obtain detailed information on the interlayer water structure. Hydrogen/deuterium substitution allows us to obtain radial distribution functions describing the environment of interlayer water molecules without recourse to the approximate differencing methods that we have applied in previous studies. For the two-layer Li−montmorillonite hydrates studied here there is no evidence for disruption of hydrogen bonding in the interlayer due to interactions with the clay surface. In future studies we will consider the one-layer hydrates, where the constraints imposed by the clay surface are more severe. Cation isotopic substitution allows us to obtain the radial distribution around the interlayer cations. The quality of the data here is insufficient to allow us to determine whether the Li^+ ions are fully hydrated or partially coordinated to the clay surface. The results do, however, give us confidence that careful experimentation will allow such information to be obtained for ions that have isotopes with a large spread of neutron scattering lengths (e.g., Ni^{2+} and Dy^{3+}).

Acknowledgment. We thank the Swiss National Science Foundation (Grants 21-49280.96 and 2124-045100.95) and the EPSRC for financial support and the Institut Laue Langevin for neutron beam time and technical support.

References and Notes

(1) Haddix, G.W.; Narayana, M. In *NMR Techniques in Catalysis*; Bell, A. T., Pines, A., Eds.; Dekker: New York, 1994.

(2) Newman, A. C. D. *Chemistry of Clays and Clay Minerals*; Longman, U.K., 1987.

(3) McCabe, R. W. In *Inorganic Materials*; Bruce, D.W., O'Hare, D., Eds.; Wiley: Chichester, 1992.

(4) Austin, G. S. *New Mexico Geology* 1986, 79−82.

(5) Boek, E. S.; Coveney, P. V.; Skipper, N. T. *J. Am. Chem. Soc.* **1995**, *117*, 12608−12617.

(6) Chang, F.-R. C.; Skipper, N. T.; Sposito, G. *Langmuir* **1995**, *11*, 2734−2741.

(7) Karaborni, S.; Smit, B.; Heidug, W.; Urai, J.; van Oort, E. *Science* **1996**, *271*, 1102−1104.

(8) Chang, F.-R. C.; Skipper, N. T. *Langmuir* **1997**, *13*, 2074−2082.

(9) Skipper, N. T.; Soper, A. K.; McConnell, J. D. C. *J. Chem. Phys.* **1991**, *94*, 5751−5760.

(10) Skipper, N. T.; Soper, A. K.; Smalley, M. V. *J. Phys. Chem.* **1994**, *98*, 942−945.

(11) Skipper, N. T.; Smalley, M. V.; Williams, G. D.; Soper, A. K.; Thompson, C. H. *J. Phys. Chem.* **1995**, *99*, 14201−14204.

(12) Powell, D. H.; Tongkhao, K.; Kennedy, S. J.; Slade, P. G. *Clays Clay Miner.* **1997**, *45*, 290−294.

(13) Powell, D. H.; Tongkhao, K.; Kennedy, S. J.; Slade, P. G. *Phys. B* **1998**, *241−243*, 387−389.

(14) Cases, J.M.; Bérend, I.; François, M.; Uriot, J. P.; Michot, L. J.; Thomas, F. *Clays Clay Miner.* **1997**, *45*, 8−22.

(15) Paalman, H. H.; Pings, C. J. *J. Appl. Phys.* **1962**, *33*, 2635−2639.

(16) Blech, I. A.; Averbach, B. L. *Phys. Rev.* **1965**, *137*, A1113−1116.

(17) North, D. M.; Enderby, J. E.; Egelstaff, P. A. *J. Phys. C* **1968**, *1*, 784−794.

(18) Sears, V. F. *Neutron News* **1992**, *3*, 26−37.

(19) Hughes, D. J.; Harvey, J. F. *Neutron Cross Sections*; McGraw-Hill: New York, 1955.

(20) Squires, G. *Introduction to the Theory of Thermal Neutron Scattering*; CUP: Cambridge, 1978.

(21) Slade, P. G.; Stone, P. A.; Radoslovich, E. W. *Clays Clay Miner.* **1985**, *33*, 51−61.

(22) Soper, A. K. In *Neutron Scattering Data Analysis 1990*; Johnson, M. W., Ed.; IOP: Bristol, 1990.

(23) Soper, A. K.; Bruni, F.; Ricci, MA. *J. Chem. Phys.* **1997**, *106*, 247−254.

(24) Dore, J. C. *J. Phys.* **1984**, *C7*, C7−C49.

(25) Cebula, D. J.; Thomas, R. K.; Middleton, S.; Ottewill, R. H.; White, J. W. *Clays Clay Miner.* **1979**, *27*, 39−52.

(26) Howell, I.; Neilson, G. W. *J. Phys.: Condens. Matter* **1996**, *8*, 4455−4463.